Electronic Supplementary Material

Unlocking wear resistance in an ultrastrong dual-phase high-entropy alloy by interface-constrained deformation of brittle Laves phases

Fei LIANG[1,†], Yixing SUN[1,†], Hongyuan WAN[2], Yong LI[1], Wenhao LU[1], Ao MENG[1], Lei GU[1], Zhaoping LUO[3], Yan LIN[1,*], Yaping ZHANG[1,*], Xiang CHEN[1,*]

[1] *Nano and Heterogeneous Materials Center, School of Materials Science and Engineering, Nanjing University of Science and Technology, Nanjing 210094, China*

[2] *Key Laboratory of Power Beam Processing, AVIC Manufacturing Technology Institute, Beijing 100024, China*

[3] *Shenyang National Laboratory for Materials Science, Institute of Metal Research, Chinese Academy of Sciences, Shenyang 110016, China*

Supporting information to https://doi.org/10.1007/s40544-024-0884-5

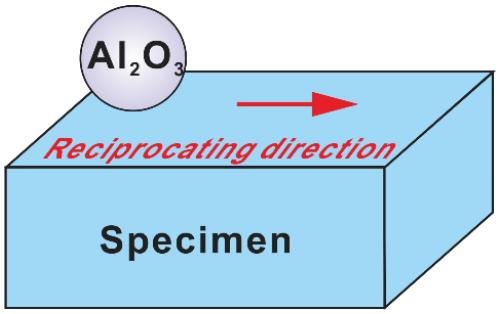

Fig. S1 Schematic illustration of the friction testing system.

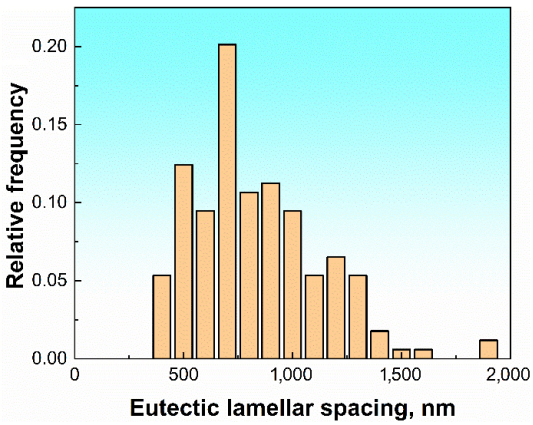

Fig. S2 Statistic distribution of the lamellar spacing within the eutectic microstructure.

† Fei LIANG and Yixing SUN contribute equally to this work.

* Corresponding authors: Yan LIN, E-mail: ylin12s@alum.imr.ac.cn; Yaping ZHANG, E-mail: yaping.zhang@njust.edu.cn; Xiang CHEN, E-mail: xiang.chen@njust.edu.cn

Table S1 Measured element composition of our AlCoFeNiNb high-entropy alloy (HEA).

Elements	Al	Co	Fe	Ni	Nb
at%	20.6±3.4	21±1.4	17.8±1.9	23.6±2.2	17.1±4.1

Table S2 Measured elemental compositions within the B2 and Laves phases.

Phase	Element (at%)				
	Al	Co	Fe	Ni	Nb
B2	35.0±4.5	17.6±1.3	12.8±2.5	24.5±2.5	10.2±2.7
Laves	12.0±2.3	22.3±1.5	22.3±1.2	13.8±2.0	29.4±3.2

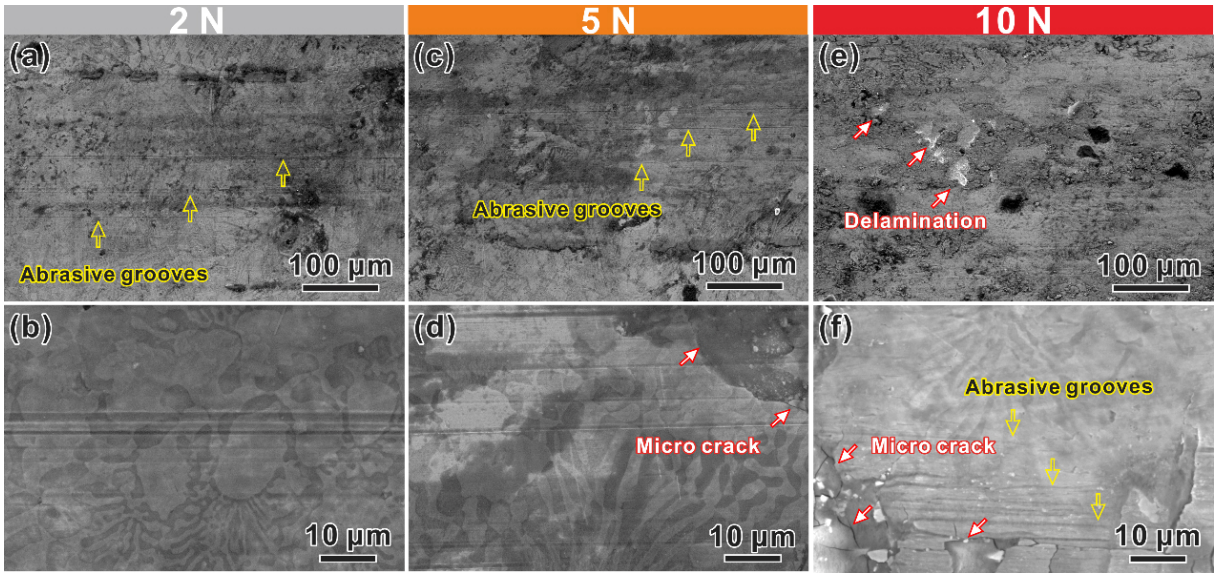

Fig. S3 scanning electron microscope (SEM) characterization of the worn surface after wear tests at room temperature under the normal load of (a, b) 2, (c, d) 5, and (e, f) 10 N.

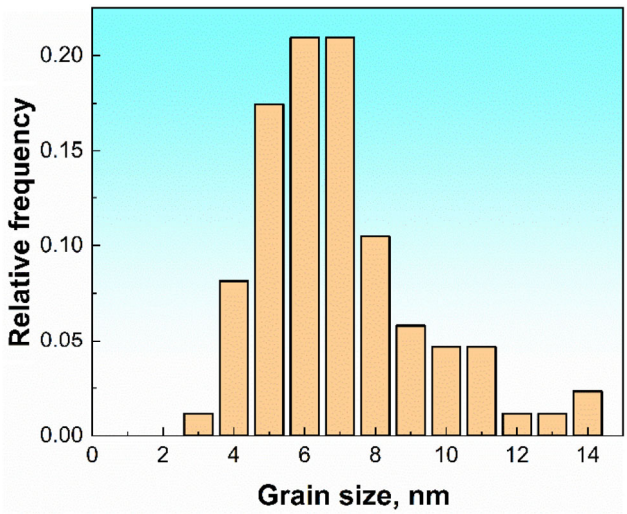

Fig. S4 Statistic distribution of the grain size in the oxidation layer formed after 9,000 cycles dry sliding at 5 N.

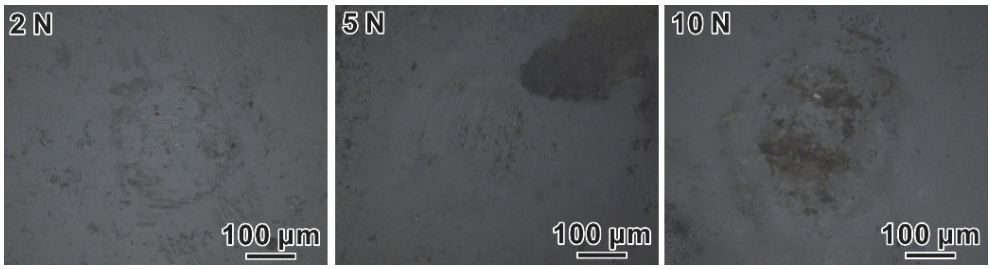

Fig. S5 Post-sliding surface morphologies of the Al_2O_3 balls after 9,000 cycles against the AlCoFeNiNb HEA under the normal loads of (a) 2, (b) 5, and (c) 10 N.

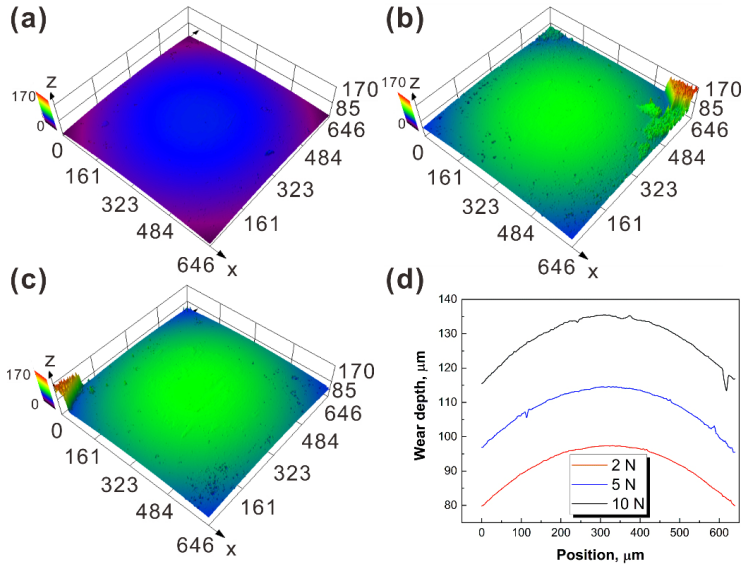

Fig. S6 Topographical area scans of the post-sliding Al_2O_3 balls' surface for 9,000 cycles against the AlCoFeNiNb HEA under the normal loads of (a) 2, (b) 5, and (c) 10 N, and the (d) representative cross-sectional wear depth plots.

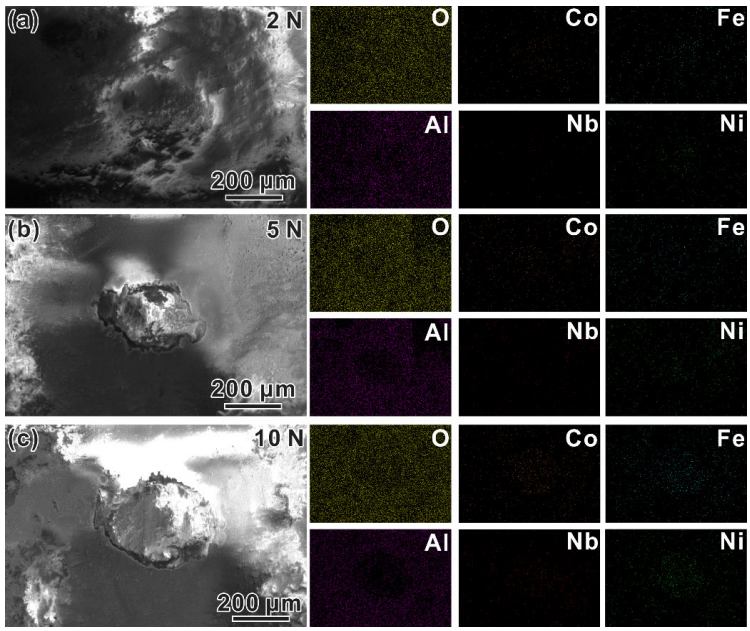

Fig. S7 Energy dispersive spectrometer (EDS) elemental mapping results of the Al_2O_3 balls' surface after 9,000 sliding cycles against the AlCoFeNiNb HEA under the normal loads of (a) 2, (b) 5, and (c) 10 N.

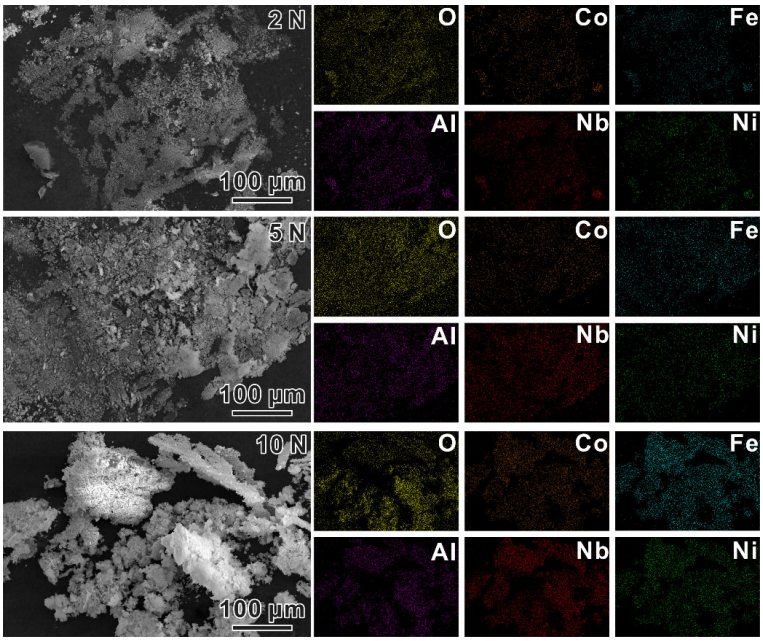

Fig. S8 SEM images and corresponding EDS elemental mapping results of the wear debris after 9,000 sliding cycles under the normal loads of (a) 2, (b) 5, and (c) 10 N.

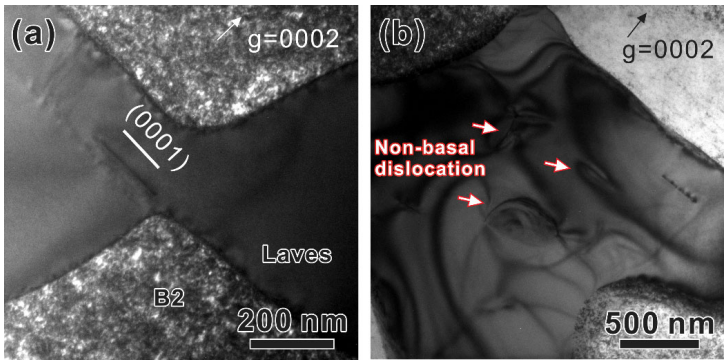

Fig. S9 Transmission electron microscopy (TEM) observation on the dislocation configurations within the B2/Laves dual-phase microstructure at the depth of (a) 0.72 and (b) 2.2 μm when viewed with g = 0002.

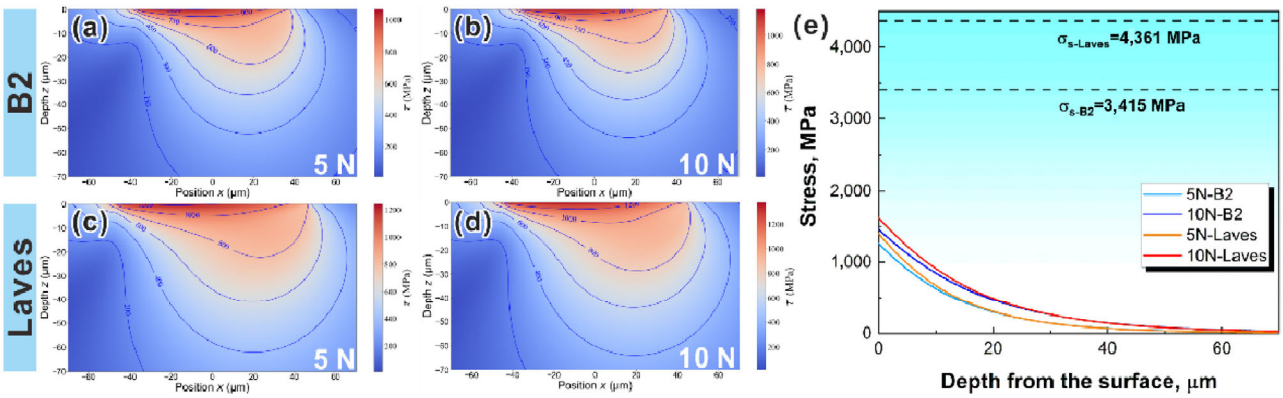

Fig. S10 σ_{xz}–component of the stress field in the middle of the wear scar for the (a, b) B2 and (c, d) Laves phases at (a, c) 5 and (b, d) 10 N. (e) Variations in applied stress at the center along depth from the sliding surface and measured yield strength along depth for the as-received B2 and Laves phases.

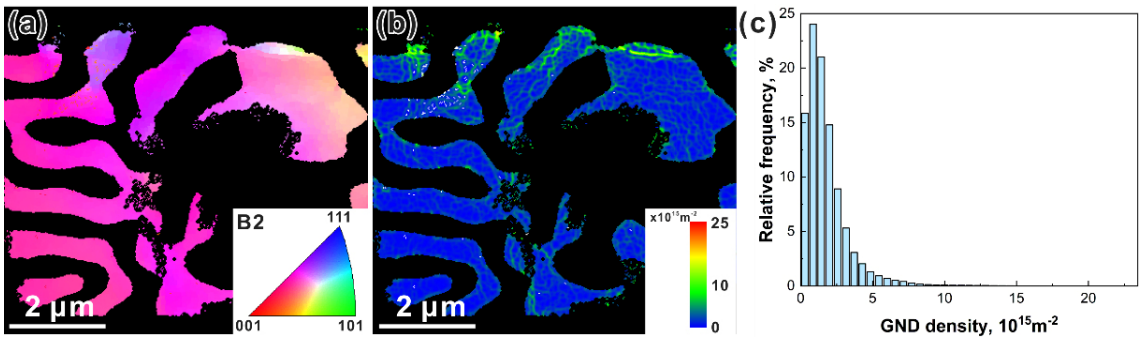

Fig. S11 (a) Orientation and (b) geometrically necessary dislocation (GND) density maps of the worn subsurface for the AlCoFeNiNb HEA during dry sliding after 9,000 cycles at 10 N. (c) Global GND density distribution on the corresponding mapping results.

Since that the Kikuchi and electron diffraction patterns of our focused ion beam (FIB)-TEM sample are relatively weak, the misorientation angles across the micro shear bands cannot be accurately measured by the electron back-scattered diffraction system (EBSD) and precession electron diffraction methods. Thus, we choose to tilt the two target regions in the Laves phases to the $[11\bar{2}0]$ zone axis and record the work angles of the TEM table as (X_1, Y_1) and (X_2, Y_2). For the B2 phases, $[11\bar{3}]$ zone axis is selected. Then, the inclination angle (ψ) between the two target regions along the $[11\bar{2}0]$ or $[11\bar{3}]$ zone axis could be obtained by:

$$\cos\psi = \cos(X_2 - X_1)\cdot\cos(Y_2 - Y_1) \tag{1}$$

For the regions on both sides of the dashed line in Fig. 4(c) in the main manuscript, the work angles of TEM table were recorded as (11.81°, -10.72°) and (1.11°, -11.16°). It is evident that there exists a rotation along the X axis between the regions on both sides of the dashed line. From a spatial perspective, the direction of X axis is parallel to the normal direction in Fig. 4 here. Thus, it is speculated that the entire Laves lamellae above the micro shear band under grain rotation along the normal direction with respect to the bulk.